

The Equilibrium Response of Atmospheric Machine-Learning Models to Uniform Sea Surface Temperature Warming

Bosong Zhang^{1*} and Timothy M. Merlis¹

¹Program in Atmospheric and Oceanic Sciences, Princeton University, Princeton, NJ

arXiv:2510.02415v2 [physics.ao-ph] 8 Jan 2026

*300 Forrester Rd, Princeton, NJ 08540

Corresponding author: Bosong Zhang, bosongz@princeton.edu

Abstract

Machine learning models for the global atmosphere that are capable of producing stable, multi-year simulations of Earth’s climate have recently been developed. However, the ability of these ML models to generalize beyond the training distribution remains an open question. In this study, we evaluate the climate response of several state-of-the-art ML models (ACE2-ERA5, NeuralGCM, and cBottle) to a uniform sea surface temperature warming, a widely used benchmark for evaluating climate change. We assess each ML model’s performance relative to a physics-based general circulation model (NOAA’s Geophysical Fluid Dynamics Laboratory AM4) across key diagnostics, including surface air temperature, precipitation, temperature and wind profiles, and top-of-atmosphere radiation. While the ML models reproduce key aspects of the physical model response, particularly the response of precipitation, some exhibit notable departures from robust physical responses, including radiative responses and land region warming. Our results highlight the promise and current limitations of ML models for climate change applications and suggest that further improvements are needed for robust out-of-sample generalization.

Introduction

A variety of machine learning (ML) approaches have been developed for weather and climate science. Substantial progress has been made in ML-based weather prediction, where forecast skill scores are now competitive with, and in some cases surpass, those of state-of-the-art numerical weather prediction models used by leading forecasting centers (Lam et al., 2023; Bi et al., 2023; Rasp et al., 2024; Keisler, 2022). A key advantage of ML models is their computational efficiency, with costs that are a fraction of those required by traditional, physical numerical weather prediction models.

Extending ML approaches to climate-timescale atmospheric modeling, however, presents additional challenges. These include the need for stable inference over periods much longer than the training data (e.g., centuries rather than decades) and the ability to generalize to climate states outside the training distribution (e.g., levels of warming not yet observed but expected in the coming century), which could potentially be addressed by incorporating physical knowledge into ML models (Beucler et al., 2024). Despite these challenges, ML may be central to the next generation of multiscale climate modeling for mitigation and adaptation strategies (Eyring et al., 2024). At a minimum, it is one component of the emerging future of climate modeling (Bordoni et al., 2025).

An important appeal of ML methods is the potential to exploit the reduced computational cost to refine climate models without requiring higher spatial resolution (Eyring et al., 2024). ML approaches can help capture essential Earth system processes and feedbacks, while remaining efficient enough to generate the large ensembles needed to study internal variability, extremes, and climate attribution. Recently, Bracco et al. (2025) reviewed advances in applying ML to the physics of climate. Overall, ML offers the potential to reduce computational cost, improve accuracy (e.g., via observational calibration), and enable the generation of very large ensembles for climate simulations.

One ML approach to atmospheric modeling is a hybrid modeling approach, where ML is used in combination with physical components. This can take the form of replacing parameterizations with ML schemes or learning the tendencies from a higher resolution model to use at lower resolution (Bretherton et al., 2022). An end-member of this approach is to retain the dynamical core and explicitly simulate large-scale atmospheric flows and replace all parameterizations of physical processes (in particular, the atmospheric water cycle and radiative transfer) with learned physics (Kochkov et al., 2024).

Alternatively, ML architectures can be trained to emulate the whole general circulation model, which has been done for both the atmosphere and ocean (Watt-Meyer

et al., 2023; Dheeshjith et al., 2025; Clark et al., 2024). To achieve stable whole model emulators, conservation blocks in the architecture ensure key physical properties such as conservation of atmospheric mass or water vapor are respected in the training process (Watt-Meyer et al., 2025; Chapman et al., 2025).

In climate change research, a fundamental benchmark is the atmospheric response to uniform sea surface temperature (SST) warming (Cess et al., 1990; Eyring et al., 2016; Merlis et al., 2024). This simple sensitivity test provides a useful standard for evaluating a model’s climate sensitivity. Diagnostics such as top-of-atmosphere (TOA) radiation balance, mean and extreme precipitation, vertical temperature profiles, and large-scale circulation responses capture essential physical processes and sensitivities underlying climate projections. This is a valuable component test of atmospheric models as it is simple to set up, rapidly equilibrates, and has well understood changes that capture the leading-order behavior of the atmospheric response to warming.

In this study, we perform a model intercomparison and evaluate the climate responses of three ML-based models—cBottle (Brenowitz et al., 2025), ACE2-ERA5 (Watt-Meyer et al., 2025), and NeuralGCM (Yuval et al., 2024)—to a uniform +2 K SST warming scenario. A limited evaluation of SST warming was presented in the ACE2 and NeuralGCM documentation papers (Watt-Meyer et al., 2025; Yuval et al., 2024). Brief descriptions of these ML models are provided in the Methods section. Their performance is compared with the Geophysical Fluid Dynamics Laboratory’s AM4 (Zhao et al., 2018a, 2018b), which serves as a physically based reference. Our analysis focuses on land surface warming patterns, hydrological changes, zonal-mean temperature and wind structures, and radiative responses under idealized warming. The output variables of the public releases of the ML models are not exhaustive, so models are omitted from the analysis as necessary. Through this intercomparison, we assess the strengths and limitations of current ML models and their potential role in future climate applications.

Response to Uniform SST Warming

Surface Air Temperature

Overall, all ML models reproduce the mean climatology of surface air temperature reasonably well compared with AM4 and the European Centre for Medium-Range Weather Forecasts’ ERA5 reanalysis (Fig. 1a-e). NeuralGCM does not provide surface air temperature directly; instead, we use the 1000 hPa air temperature as a proxy, so its high-altitude regions are not comparable, as the temperature there includes subsurface extrapolation. The global-mean surface air temperatures, indicated above the maps in Fig. 1, are close to that of ERA5 for all models.

In response to uniform SST warming, AM4 exhibits pronounced land warming (Fig. 1h), which is a well-understood result of enhanced surface warming over dry surfaces because of the relationship between relative humidity near the surface and the atmospheric lapse rate (Joshi et al., 2008; Byrne & O’Gorman, 2013a, 2013b). This amplified warming over land is underestimated in cBottle (Fig. 1f). Nonetheless, cBottle simulates amplified polar warming, likely due to sea-ice loss induced by SST warming (not shown). Notably, sea ice is an output in cBottle, making it slightly different from conventional atmosphere-only simulations with prescribed SST and sea ice. In contrast, ACE2 shows a surface air temperature response over land that is a mix of warming and cooling (Fig. 1g)—a limitation also noted by Watt-Meyer et al. (2025). Enhanced land warming is well captured in NeuralGCM compared to AM4, although the magnitude of polar warming is underestimated (Fig. 1i). This is suggestive of an important role for NeuralGCM’s dynamical core in capturing the land-sea mechanism (Byrne & O’Gorman, 2013a) that posits weak temperature gradients aloft and differences in lower-tropospheric lapse rate set the amplitude of land enhanced warming. While ACE2-ERA5 does not have enhanced land

Surface Air Temperature

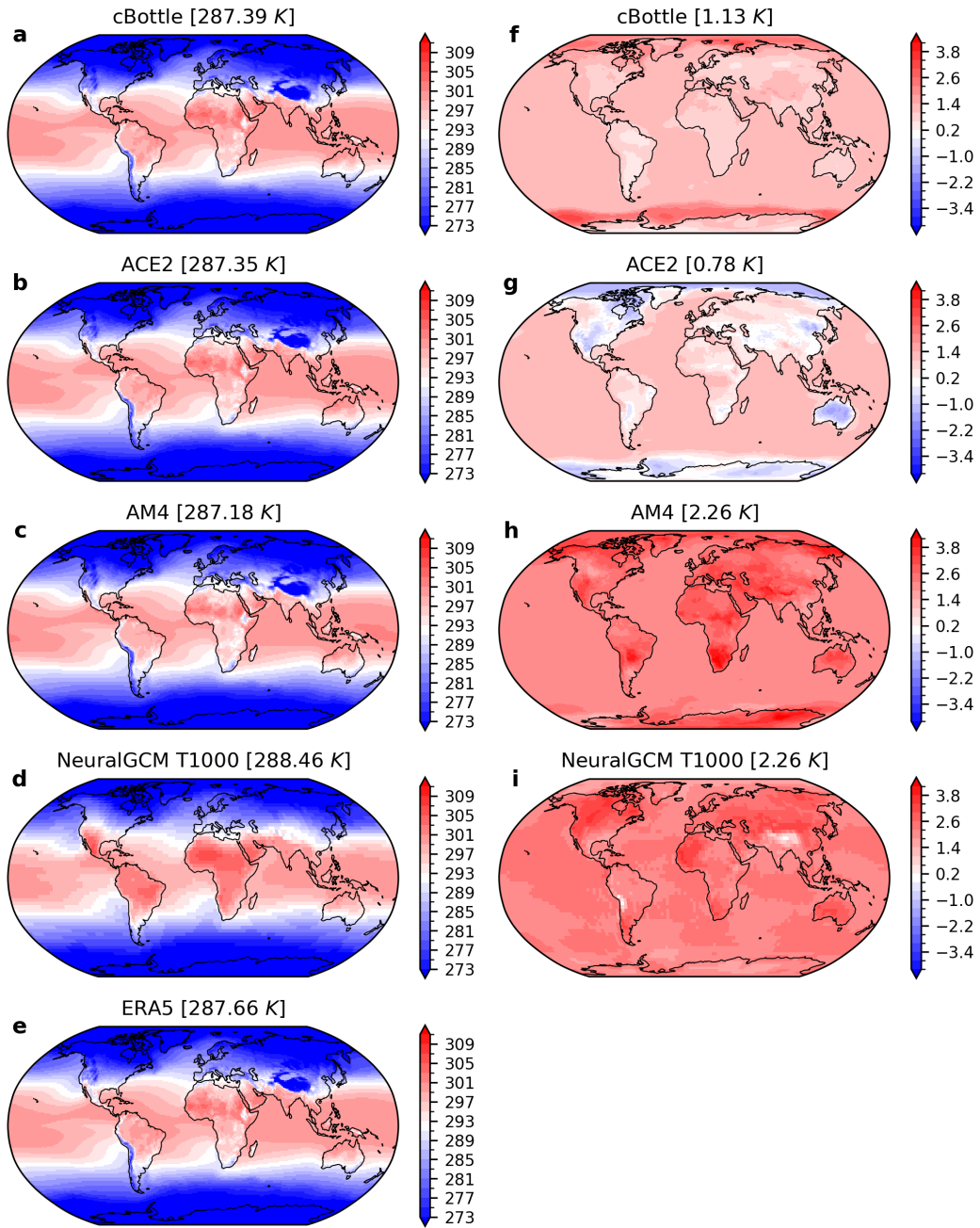


Figure 1. Annual mean surface air temperature for (left) the climatology and (right) the response to a uniform +2 K SST perturbation for cBottle, ACE2, AM4, and NeuralGCM from top to bottom. ERA5 is included in panel (e) for reference of the mean state. Note that NeuralGCM does not directly output surface air temperature. Here we use temperature at 1000 hPa to illustrate the temperature pattern near the surface.

warming, ACE2 does have enhanced land warming when trained across physical model simulations of multiple climates (Clark et al., 2024).

The land-enhanced warming in AM4 and other General Circulation Models (GCMs) means that the global-mean surface air temperature exceeds that of the imposed SST perturbation. This is the case for the 1000 hPa temperature in NeuralGCM, but both ACE2 and cBottle have less global-mean surface air temperature change than the imposed SST increase. Beyond the land response, the ocean region response can also contribute. In particular, we find that cBottle has SST and surface air temperature increases over the ocean that are less than the imposed 2 K perturbation. Analogous cold biases have been documented in ML-based weather forecasts for years beyond the end of the training period, as there has been additional warming that the models do not generalize to (Rackow et al., 2024; Landsberg & Barnes, 2025).

Precipitation

The mean climatology of precipitation is reasonably well captured by all models (Fig. 2a-e). The global-mean precipitation simulated by cBottle, ACE2, and AM4 agrees closely with observed estimates from the GPCP dataset, while NeuralGCM produces slightly higher values (Fig. 2).

Under uniform SST warming, all models simulate an increase in global-mean precipitation, with the strongest regional increases in the tropics (Fig. 2f-h). The magnitude of the global-mean precipitation change is quantitatively similar to the GCM shown here and the robustly simulated magnitude of a $\approx 3\% \text{ K}^{-1}$ increase that is driven by increased radiative cooling (Allen & Ingram, 2002; Jeevanjee & Romps, 2018). One regional discrepancy is cBottle’s weak increase in northern hemisphere mid-latitude. There are regions in the low latitudes, particularly over land and the subtropical oceans, where the GCM response is a decrease in precipitation and the ML models show similar behavior to varying degrees. This is broadly consistent with the thermodynamic, “wet-get-wetter, dry-get-drier” response (Held & Soden, 2006), which we evaluate next.

Precipitation minus evaporation (P–E) is governed by the vertically integrated water vapor transport, which has thermodynamic increases under warming because the saturation vapor pressure of air increases with temperature according to the Clausius-Clapeyron relation (Held & Soden, 2006). We show changes in P–E in Fig. 3. The evaporation field is unavailable in cBottle, so it is excluded. ACE2, NeuralGCM, and AM4 all exhibit the canonical “wet-get-wetter, dry-get-drier” response (Held & Soden, 2006), with increased P–E along the Intertropical Convergence Zone (ITCZ), reduced P–E in subtropical subsidence regions, and increased P–E in the extratropics (Fig. 3). In addition, these models show deviations from the thermodynamic response approximated by $\alpha\Delta T(\bar{P} - \bar{E})$ (dashed lines in Fig. 3), including a poleward expansion of subtropical dry zones. This is an impressive degree of agreement with physical models for a non-trivial aspect of the response to warming.

It is interesting and surprising that these ML models generalize the precipitation rate to warmed atmospheres. This raises the question of what aspects of today’s climate, as encapsulated in the ERA5 training dataset, give rise to this behavior. While it is a challenge to interpret large neural networks (e.g., ACE2 has 450 million parameters), we think it is useful to consider intervariable relationships that are known to be important in physical models. First, the specific humidity q of historical atmospheric states is constrained by the Clausius-Clapeyron relation that governs the saturation vapor pressure: $q \leq q^*(T, p)$, where $q^*(T, p)$ is the temperature and pressure-dependent saturation specific humidity. A thermodynamic increase in humidity with warming is embedded in today’s atmospheric state. Second, a relationship between humidity and precipitation rates would allow for the warmer temperatures to translate to precipitation changes.

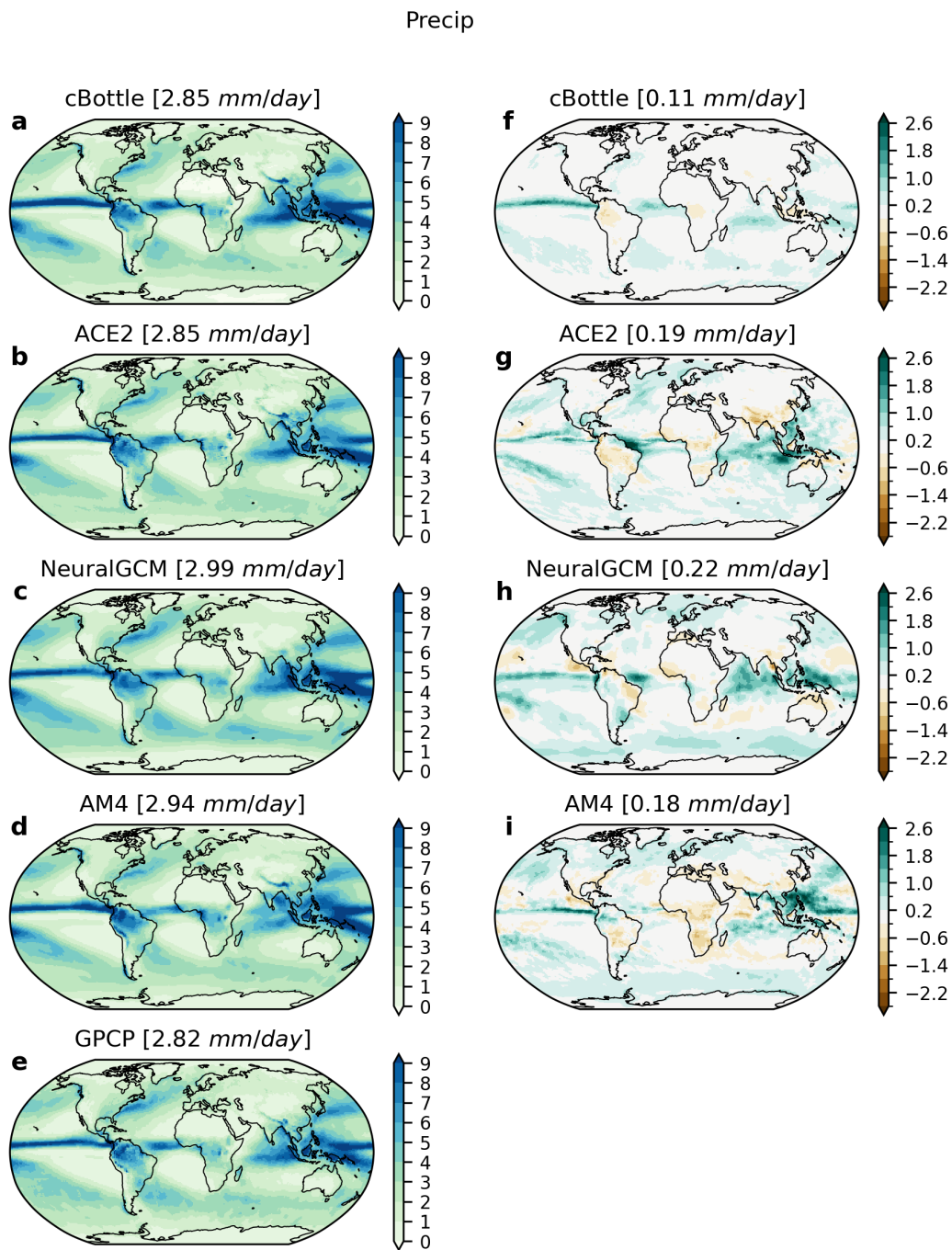


Figure 2. Annual mean precipitation for (left) the climatology and (right) the response to a uniform +2 K SST perturbation for cBottle, ACE2, NeuralGCM and AM4, from top to bottom. GPCP is included in panel (e) for reference.

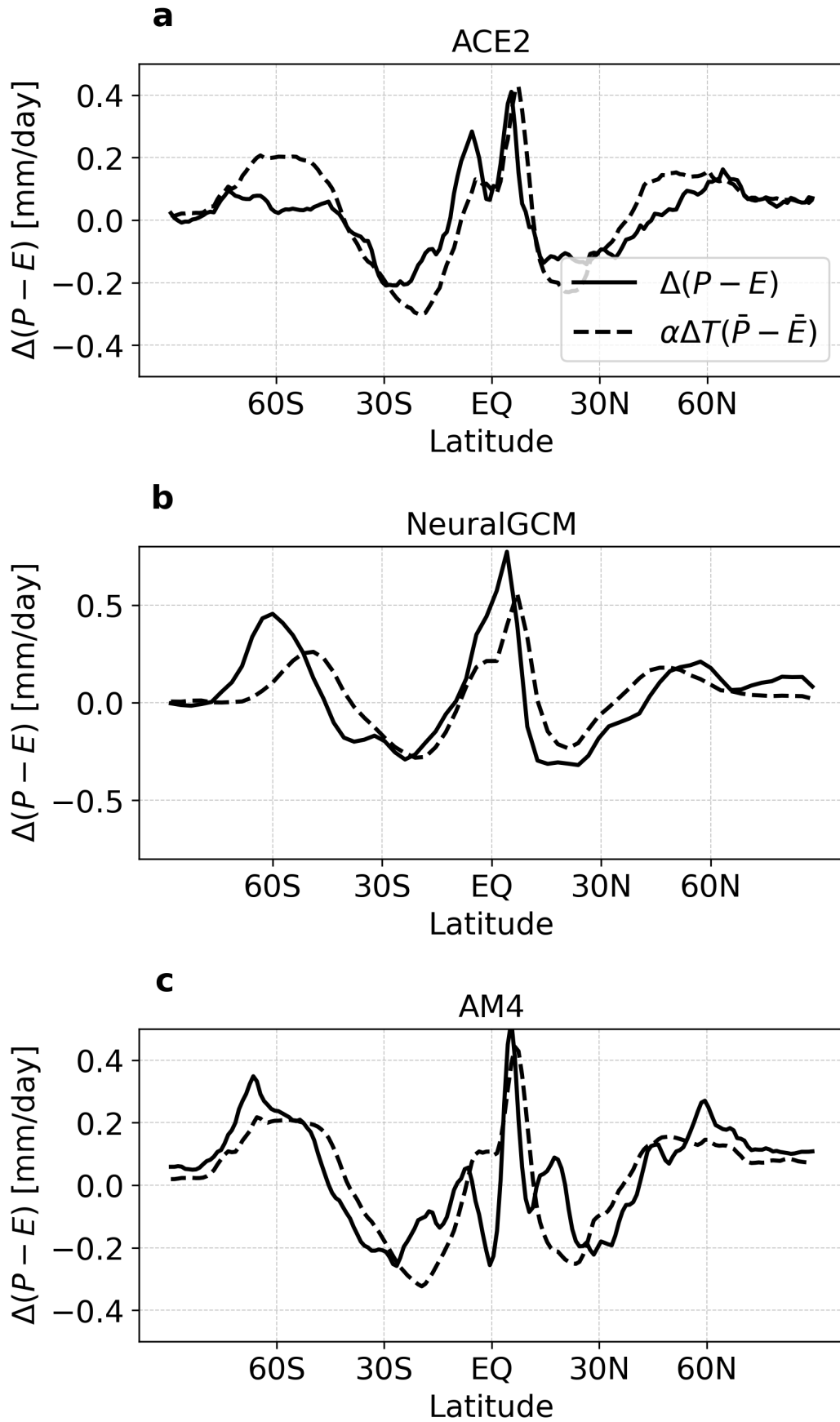


Figure 3. The zonal mean change of precipitation minus evaporation for ACE2, NeuralGCM and AM4 from top to bottom. The dashed lines in each panel is the thermodynamic component, approximated as $\alpha\Delta T(\bar{P} - \bar{E})$ with $\Delta T = 2\text{K}$ and $\alpha = 0.07\text{K}^{-1}$.

With this interpretative lens, we analyze the relationship between daily mean precipitation and column water vapor (CWV) in the tropics (Bretherton et al., 2004; Kuo et al., 2020; Neelin et al., 2022). There is typically weak precipitation until a sufficiently high value of CWV ≈ 50 mm, where there is a transition to a sensitive increase in precipitation with CWV (Bretherton et al., 2004). All of the models capture some form of this climatological precipitation–CWV relationship (Fig. 4). With SST warming, the precipitation “onset” value of CWV increases. Physically, this is expected because the saturation deficit increases with warming if the relative humidity is approximately unchanged. At the highest values of CWV, particularly those that exceed the maxima of the control climate, the precipitation associated with the highest CWV bins becomes stronger. All ML models have some shift in the physically expected direction, although the degree to which the onset CWV shifts to higher values varies between the ML models, with the ≈ 10 mm of NeuralGCM most comparable to AM4. At the highest CWV bin, all models have an increase in the precipitation rate, though all ML models have a weaker increase than AM4. In summary, it appears that there are compensating errors in the changes in the precipitation–CWV relationship in the perturbed climates: the modest shift in onset of strong precipitation tending to increase the mean precipitation more than physical models, but the weaker increase in precipitation at the highest CWV mutes the increase.

We also examine extreme precipitation, using the 99.9th percentile of daily precipitation at each grid point, following O’Gorman and Schneider (2009b, 2009a). The zonal mean of this metric is shown in Fig. 5. There are substantial differences in the magnitude of the control precipitation extremes, with cBottle having the smallest values. ACE2’s magnitude of ≈ 50 mm day $^{-1}$ in the tropics is similar to the ERA5 data on which it was trained. The ML models capture the equator-to-pole contrast in the precipitation extremes, though ACE2 has locally suppressed extremes near the equator.

Under uniform SST warming, extreme precipitation intensifies across all models (Fig. 5). The structure of the extremes in the warmed climate largely follows that of the control, with increases in the tropics (30°S to 30°N) that are $\approx 4.5\%$ K $^{-1}$ for cBottle, $\approx 3.1\%$ K $^{-1}$ for ACE2, $\approx 3.8\%$ K $^{-1}$ for NeuralGCM, and $\approx 4.6\%$ K $^{-1}$ for AM4. These changes are smaller than that estimated by the Clausius-Clapeyron relationship of saturation vapor pressure of about 6-7 % K $^{-1}$.

Atmospheric Temperature and Circulation Response

The climatological zonal-mean temperature profiles are shown in the left column of Fig. 6. The temperature distribution is reasonable across all models, with a tropical tropospheric temperature maximum that decreases poleward.

In response to SST warming, AM4 exhibits pronounced upper-tropospheric warming in the tropics (Fig. 6h), consistent with moist adiabatic adjustment driven by increased latent heat release from deep convection (Santer et al., 2005). This amplified warming is well reproduced by NeuralGCM (Fig. 6g) but is substantially weaker in both cBottle and ACE2 (Figs. 6e and f), where the upper-tropospheric warming is similar to the near surface-temperature response in the tropics.

The closer agreement between NeuralGCM and AM4 may reflect the role of a dynamical core in both models, which is absent in cBottle and ACE2, or may reflect differences in its training approach. NeuralGCM simulates notable stratospheric cooling under uniform SST warming (Fig. 6g), whereas the other models show little to no such signal. Stratospheric cooling in warmed climates is dominated by temperature adjustments to carbon dioxide forcing (rather than being proportional to the SST warming), and ACE2 captures this when trained on physical model simulations that have a slab ocean boundary condition and perturbed carbon dioxide concentration (Clark et al., 2024).

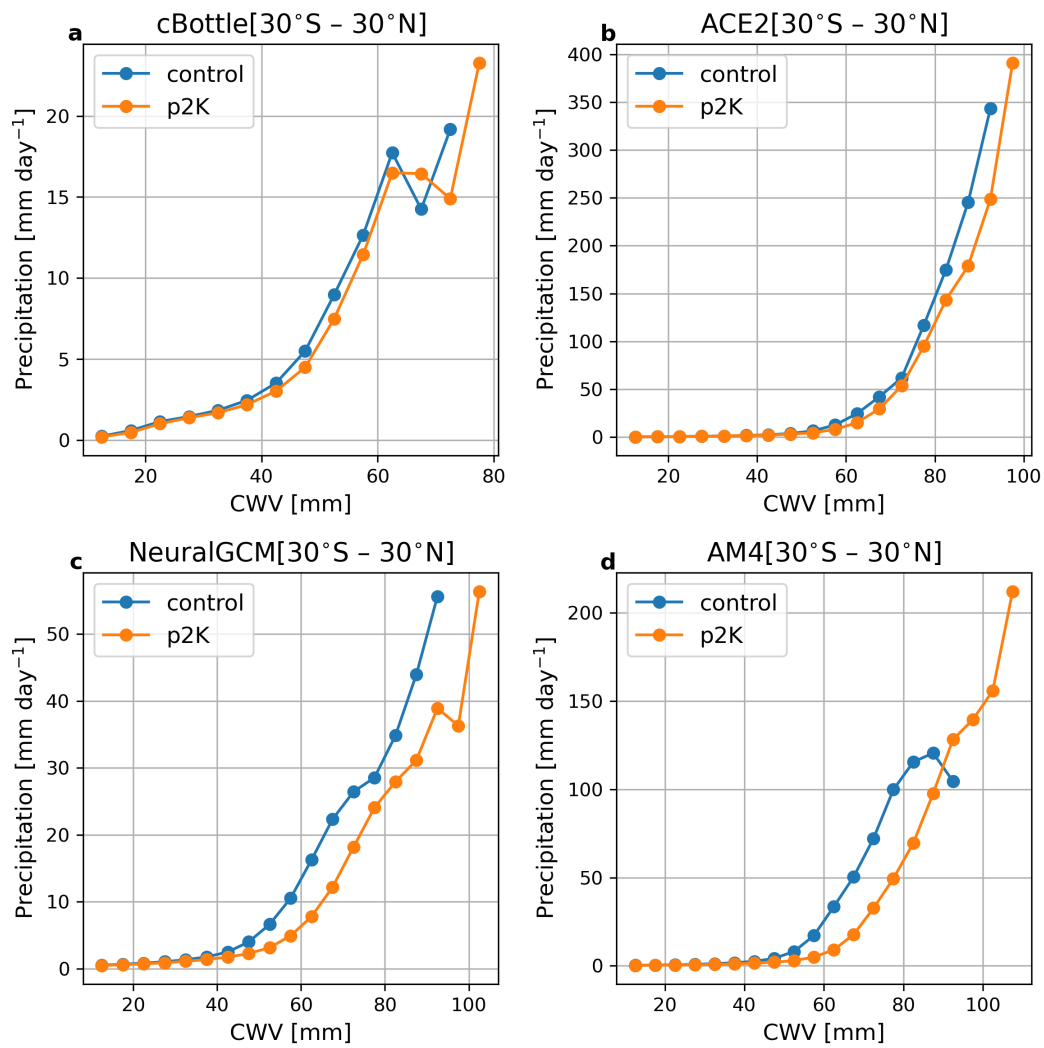


Figure 4. Daily mean precipitation vs binned column water vapor in the tropics (30°S–30°N) for (a) cBottle, (b) ACE2, (c) NeuralGCM, and (d) AM4 for the control simulation (blue) and the +2K simulation (orange).

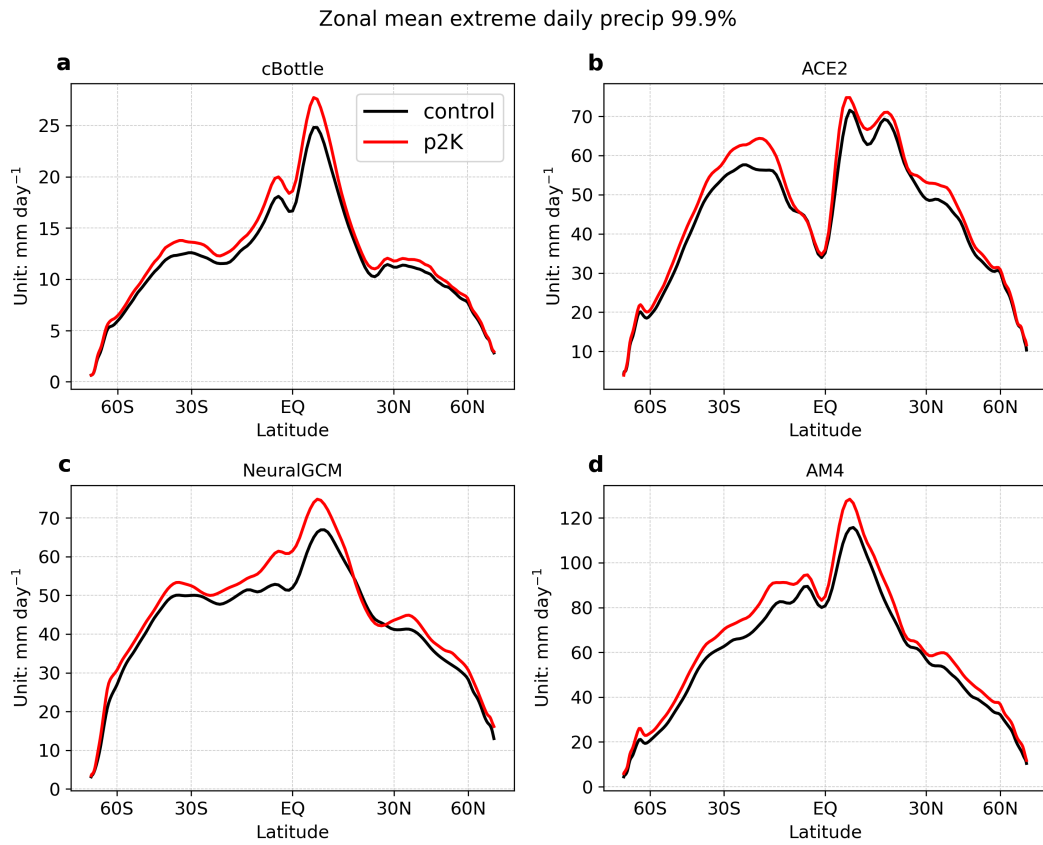


Figure 5. Zonal mean 99.9th percentile of daily precipitation for (a) cBottle, (b) ACE2, (c) NeuralGCM, and (d) AM4. Results are shown for the control simulation (black) and the +2K simulation (red).

Temperature

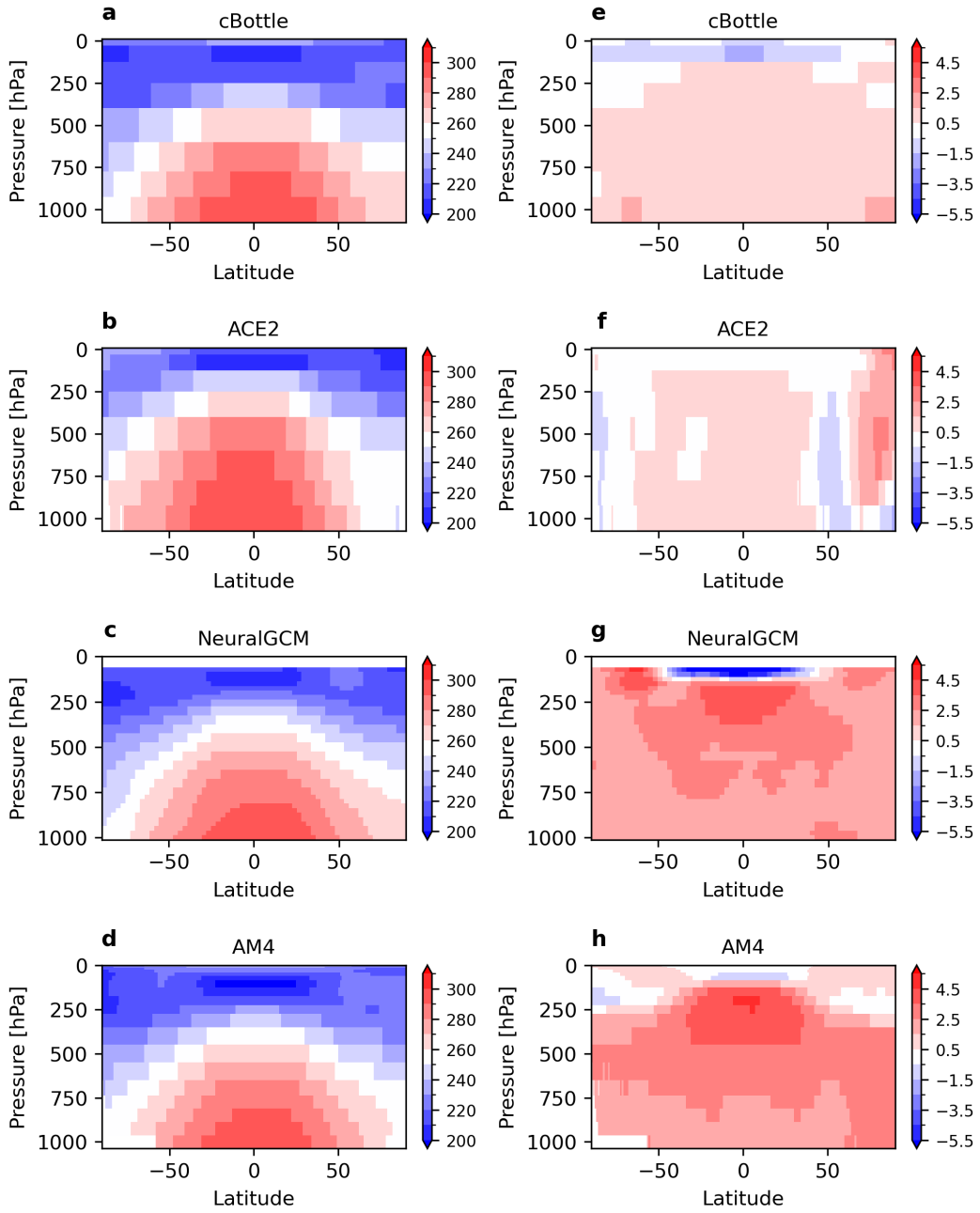


Figure 6. Annual- and zonal-mean (left) control simulation temperature and (right) temperature response to +2K SST warming of (a,e) cBottle, (b,f) ACE2, (c,g) NeuralGCM, and (d,h) AM4. Note that pressure levels below 40 hPa are masked out for NeuralGCM because the model top corresponds to $p/p_s = 0.03$ (Kochkov et al., 2024).

Similar to temperature, the climatological zonal-mean zonal wind is realistically captured by all models, featuring upper-tropospheric westerly jets in both hemispheres and tropical easterlies. One climatological bias is the width of the westerly jet in the southern hemisphere extratropics in ACE2, which occupies a narrower range of latitudes (Fig. 7d). A more detailed assessment of the variability of the present-day atmospheric circulation in ACE2 and NeuralGCM can be found in Baxter et al. (2025).

The zonal-mean zonal wind response to SST warming differs substantially across models (Fig. 7). Overall, cBottle and ACE2 display zonal wind responses of both signs (Fig. 7e and f), with meridional structure on the scale of $\approx 10^\circ$ that do not bear clear relationships to the climatological winds. In contrast, NeuralGCM and AM4 simulate a strengthening of upper-tropospheric westerlies (Fig. 7g and h), consistent with their warming patterns aloft (Fig. 6g and h) and the thermal wind balance. AM4 has poleward shifts in the surface westerlies, a longstanding result of GCM simulations of climate change (Kushner et al., 2001). NeuralGCM and cBottle have weak changes in the surface zonal wind, while ACE2 has the narrower scale changes extending to the surface. NeuralGCM also produces anomalous stratospheric easterlies (Fig. 7g), which are absent in AM4 and are linked via thermal wind to the exaggerated stratospheric cooling in NeuralGCM (Fig. 6g).

Figure 8 shows zonal-mean meridional streamfunction. Unlike the zonal wind, the mean state of the meridional streamfunction differs substantially across models. In cBottle, the northern hemisphere Hadley cell is stronger than its southern hemisphere counterpart (Fig. 8a), while ACE2 shows clear deficiencies in simulating the Hadley circulation (Fig. 8b). This discrepancy between the climatology of the meridional wind in the ML models and Earth’s climatology suggests that the mean meridional wind is a more difficult variable to train, perhaps owing to its smaller variance in the tropics compared to the extratropics.

Under SST warming, cBottle has a strengthening of the northern hemisphere Hadley cell and a vertically varying response in the southern hemisphere, with near-surface weakening and upper tropospheric strengthening (Fig. 8a). ACE2 shows mixed signals, with changes in the sign of the streamfunction response over small meridional scales (Fig. 8b). NeuralGCM has an equatorward shift of the ITCZ (Fig. 8c) and the P-E change is physically consistent with this (Fig. 3b). AM4 exhibits a weakening of the Hadley cell in both hemispheres (Fig. 8d) by about $\approx 1\%$, which is in line with most GCMs projecting a weakening of the Hadley cell, although the magnitude is uncertain, ranging from $0\% \text{ K}^{-1}$ to $4\% \text{ K}^{-1}$ (Vecchi & Soden, 2007; D’Agostino et al., 2017; Lionello et al., 2024).

Radiation

TOA radiation is another key diagnostic of atmospheric models. NeuralGCM is excluded from this analysis because it does not provide TOA radiation fields. We first examine the mean climatology of upward shortwave (SW) radiation at TOA. cBottle slightly underestimates the global-mean upward SW flux, while ACE2 and AM4 produce global means that are closer to CERES observations (Fig. 9).

The response of upward SW radiation to SST warming varies substantially across the three models. In cBottle, the upward SW flux is strongly reduced almost everywhere except in the deep tropics (Fig. 9e). In contrast, ACE2 and AM4 show much smaller decreases in global-mean upward SW radiation—less than 1 W m^{-2} (Fig. 9f and g). A decrease in the global-mean reflected solar radiation is typical among GCMs (Merlis et al., 2024). The spatial pattern of responses differs between ACE2 and AM4, with ACE2 exhibiting positive anomalies over most land regions (except Africa) and AM4 having predominantly negative anomalies over land. We note that the SW cloud response to warming is uncertain (i.e., there is substantial intermodel spread between GCMs).

Zonal Wind

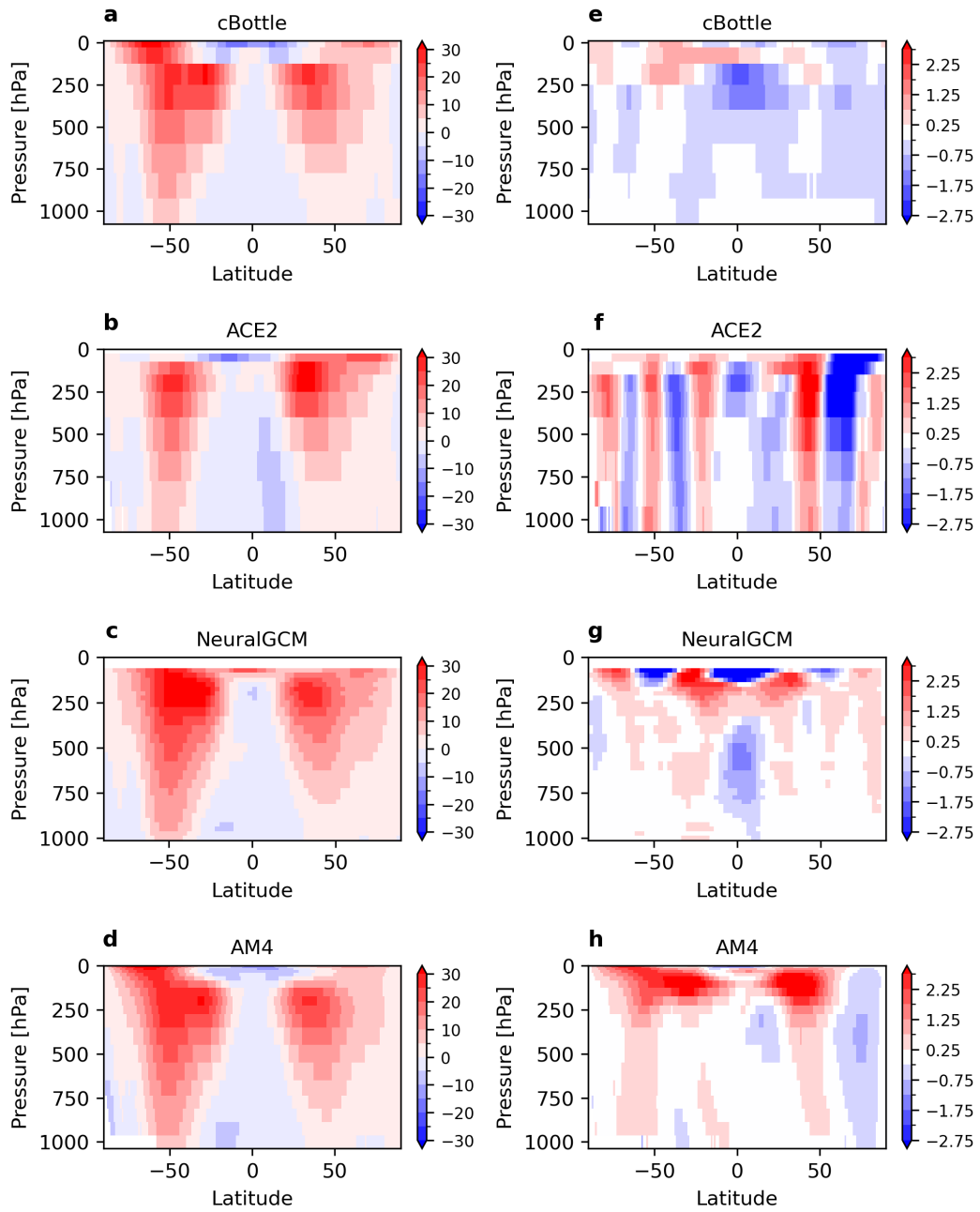


Figure 7. Annual- and zonal-mean (left) control simulation zonal wind and (right) zonal wind response to +2K SST warming of (a,e) cBottle, (b,f) ACE2, (c,g) NeuralGCM, and (d,h) AM4. As in Fig. 6, pressure levels below 40 hPa are masked out for NeuralGCM.

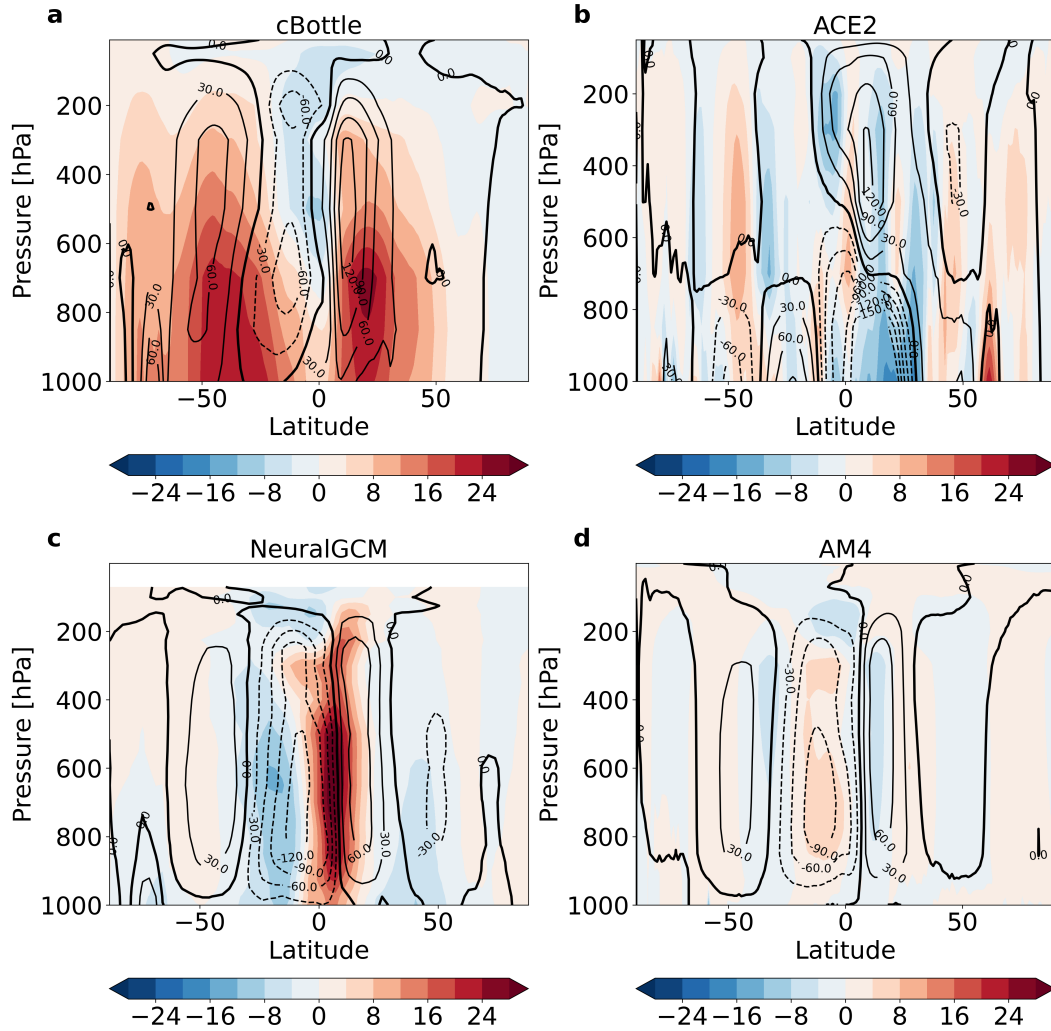


Figure 8. Annual- and zonal-mean meridional streamfunction for (a) cBottle, (b) ACE2, (c) NeuralGCM, and (d) AM4. Contours denote the climatological mean state, and shading shows the response to +2 K SST warming (p2K minus control). Contours range from 150 to 150 at intervals of 30, with the zero contour shown as a thick line. Units are $\times 10^9 \text{ kg s}^{-1}$. As in Fig. 6, pressure levels below 40 hPa are masked out for NeuralGCM.

For outgoing longwave radiation (OLR), the mean climatology in all models agrees reasonably well with observations, with global mean values near 240 W m^{-2} (Fig. 10). The basic regional features of this climatology are represented in all models: the OLR is lower in the deep tropics, where there are high clouds and high humidity, compared to the drier subtropics, and there is an equator-to-pole reduction in OLR as the emission decreases with mean temperature.

Under SST warming, the global-mean OLR increases in all models, indicating enhanced longwave cooling. However, the magnitude of this cooling tendency is weaker in both cBottle and ACE2 compared to AM4 (Fig. 10). As a result, the combined SW and LW responses in cBottle lead to a net positive energy imbalance. This is physically unrealistic, as the implied feedback parameter would produce a runaway warming if the SST were allowed to respond consistent with the energy budget changes. To shed light on the extent to which this behavior is particular to the uniform SST perturbation or is found generically in cBottle, we also conducted additional experiments in which only localized (patch) SST warming anomalies were imposed, following the Green’s function–style experiments previously performed with AM4 (Zhang et al., 2023; Bloch-Johnson et al., 2024). In this case, cBottle exhibits a negative global-mean net TOA radiation response to the SST patch warming, indicating a stable feedback (not shown). A recent study also applied Green’s-function–style experiments to the ACE2 model and found results that are physically consistent with those from traditional physics-based models (Wu et al., 2025). The contrasting behaviors between the uniform and patched SST warming experiments suggest that the idealized uniform SST warming case represents a truly out-of-sample prediction, where the model is unable to extrapolate reliably, whereas the regional patch experiments have perturbations that are closer to the model’s training distribution (e.g., historical El Niño-Southern Oscillation events).

Although ACE2 simulates a decrease in TOA net radiation under warming, its magnitude is much weaker than in AM4. In other words, AM4 exhibits a more stable climate feedback parameter than ACE2, driven primarily by larger OLR response. Normalizing the change in TOA flux by the surface-air temperature change brings ACE2 and AM4’s feedback parameter closer together because of the muted surface warming in ACE2.

The spatial pattern of the change in OLR has a common reduction in OLR over tropical deep convective regions across the models. In a physical model, one can interpret this as reflecting an expansion of high cloud area. It could also indicate higher cloud tops under warmer SSTs, though typically the cloud top temperatures are unchanged with warming (Hartmann & Larson, 2002). Scatter plots of OLR change versus climatological SST in the tropics (Fig. 11) show that negative OLR responses are consistently associated with high-SST regions, characteristic of active deep convection. Above 300 K, cBottle’s OLR response is predominantly negative, whereas ACE2 and AM4 display a mixture of positive and negative responses.

Conclusion and Discussion

We compared the mean state and climate responses to uniform SST warming in three atmospheric ML models—cBottle, ACE2, and NeuralGCM, using the physics-based AM4 GCM as a reference. Observations were also used to evaluate the mean state of each model. To first order, all ML models reproduce the observed climatology reasonably well, including air temperature, precipitation, circulation, and radiation fields. This agreement is not surprising, given that ERA5 reanalysis data were used in their training. Two aspects of the control climatology that differ across models are the Eulerian-mean mass transport (i.e., the mean meridional wind) and the extreme precipitation metric (99.9th percentile of daily precipitation rate) assessed here.

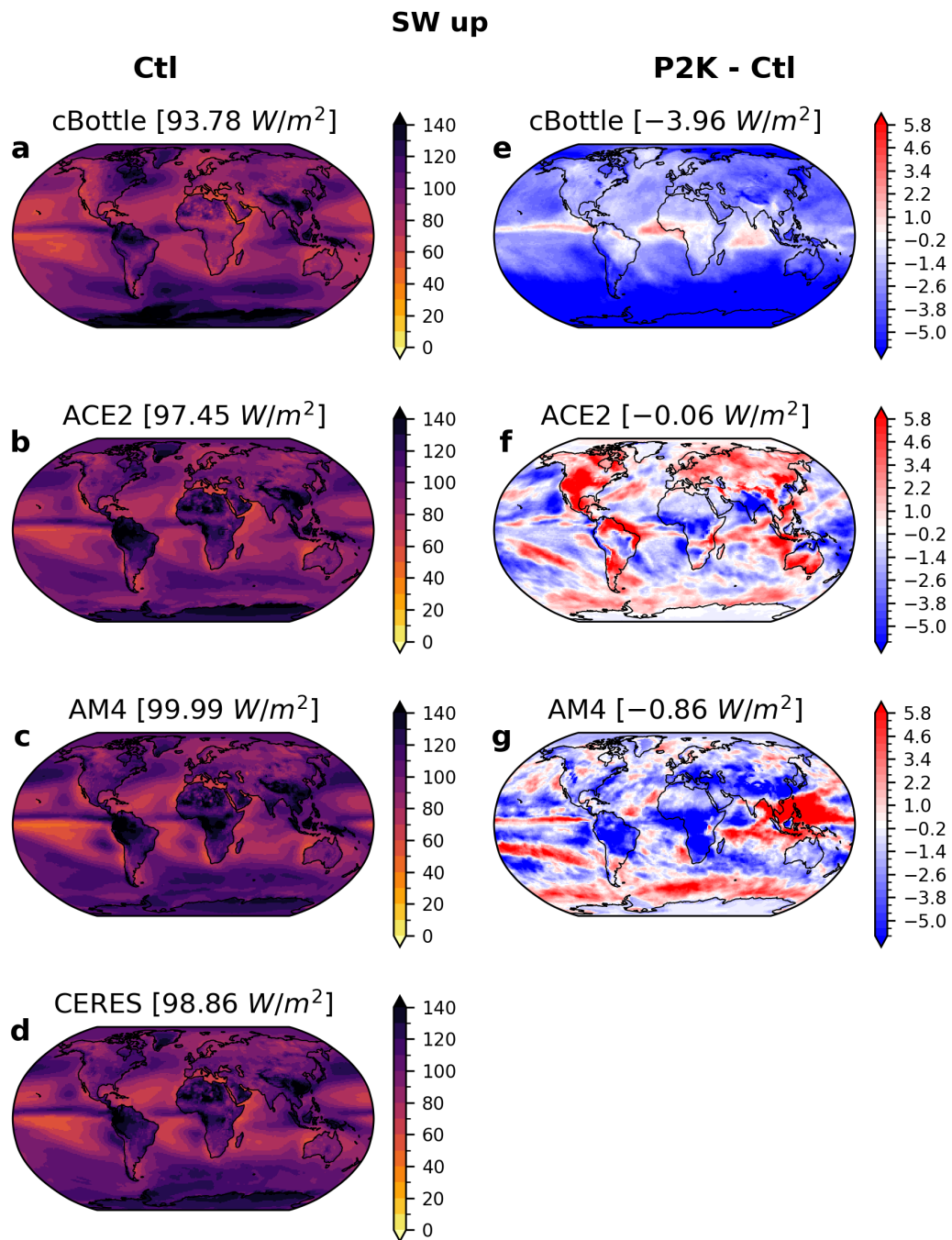


Figure 9. Annual-mean upward SW radiation at TOA for (left) the control simulation and (right) the response to +2K SST perturbation for cBottle, ACE2, and AM4 from top to bottom. CERES is shown in panel (d) for reference.

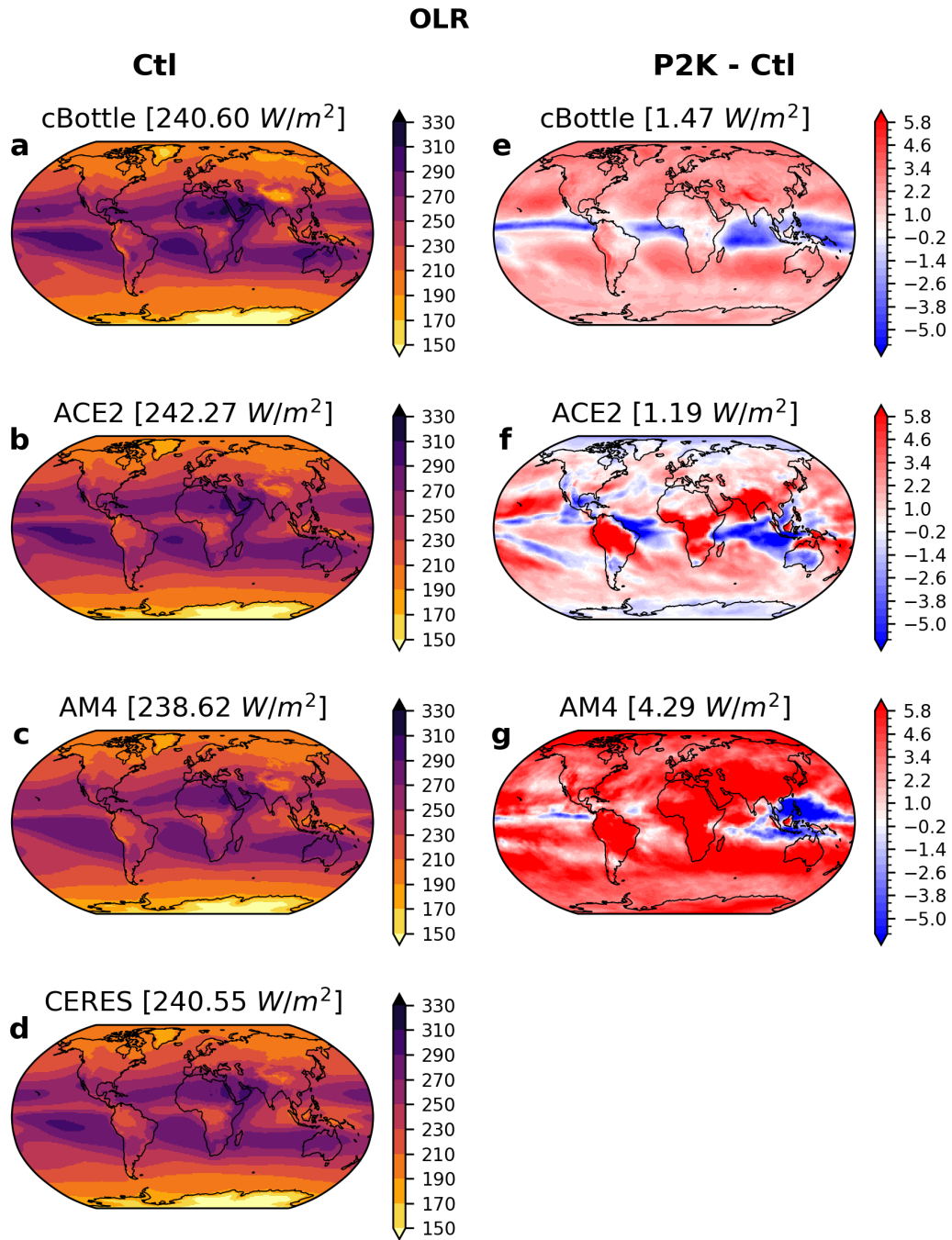


Figure 10. Annual-mean OLR at TOA for (left) the control simulation and (right) the response to +2K SST perturbation for cBottle, ACE2, and AM4 from top to bottom. CERES is shown in panel (d) for reference.

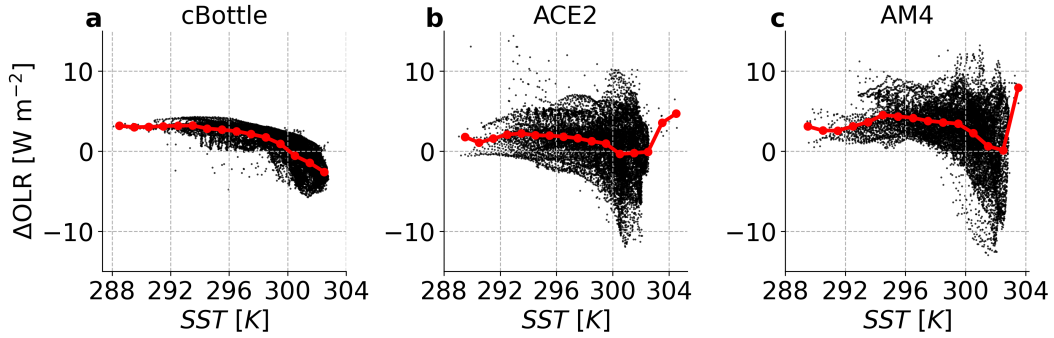


Figure 11. The response of OLR to +2K SST warming vs the control SST at each grid point (black dots) for (a) cBottle, (b) ACE2, and (c) AM4. The red solid line in each panel denotes the mean OLR response within SST bins from 288 to 305 K, using 1 K intervals.

The response to uniform SST warming provides a straightforward measure of a model’s sensitivity to external forcing. For ML models, this experiment serves as an out-of-sample test. We find the ML models exhibit substantially different responses to SST warming, including some discrepancies from well understood physical responses.

For surface air temperature, cBottle and ACE2 underestimate the overall magnitude of warming. Differences in model structure account for cBottle’s polar warming (associated with its determination of sea ice as an output of the inference). In contrast, ACE2 has high latitude cooling. Neither cBottle nor ACE2 has enhanced land surface warming, which is a robustly simulated GCM response. This issue is ameliorated when ACE2 is trained on physical model simulations of perturbed climates (Clark et al., 2024). NeuralGCM’s lowest atmospheric temperature response is enhanced over land regions, consistent with the known physical response.

The precipitation response to warming is well captured by the models assessed here. All exhibit an increase in global-mean precipitation and regional changes, such as the largest increase in the deep tropics, which are characteristic of GCM-simulated changes. Both ACE2 and NeuralGCM capture the canonical ‘wet-get-wetter, dry-get-drier’ pattern seen in AM4 and other physics-based models, resulting from thermodynamic increases in atmospheric water vapor with temperature (Held & Soden, 2006). Because the relationships among temperature, humidity, and precipitation are inherently embedded in the training data (e.g., ERA5), the ML models can reproduce the overall pattern of precipitation changes driven by increases in humidity and temperature under uniform SST warming. The strong coupling between precipitation and humidity is illustrated in Fig. 4, where all models show a rapid increase in precipitation once column water vapor exceeds approximately 50 mm. In addition, the ML models also have expansions of subtropical dry zones that are known to result from wind changes in physical models. Last, all models simulate an intensification of extreme precipitation under SST warming, though the magnitude of this response varies quantitatively.

For atmospheric temperature responses, NeuralGCM and AM4 both show amplified warming in the tropical upper troposphere, whereas cBottle and ACE2 fail to reproduce this long-standing feature of climate model simulations. Similarly, intensified upper-tropospheric westerlies are simulated by NeuralGCM and AM4, but not by cBottle and ACE2. The physical consistency—or lack thereof—in the relationship between the zonal wind and temperature change is evidence of the dynamical core in constraining the atmospheric response to SST warming, as it ensures dynamical relationships such as thermal wind balances are respected.

The meridional streamfunction changes in the ML models are much larger in magnitude than in AM4, and the spatial patterns in cBottle and ACE2 show little resemblance to either the climatological circulation or AM4’s response. This pronounced discrepancy underscores a fundamental limitation: these ML models not only misrepresent the mean meridional mass transport in the present climate but also exhibit dynamically implausible responses under warming (e.g., latitudes with net mass flux through the surface). NeuralGCM’s mean overturning circulation and its response to uniform SST warming also deviate substantially from AM4. Overall, this basic feature of the atmospheric circulation is one that warrants further attention in ML models to improve their ability to simulate realistic overturning circulations.

The radiative responses further underscore differences among the models. While ACE2 and AM4 broadly agree on the sign of radiative changes, ACE2 exhibits weaker increases in OLR than AM4. cBottle even produces an unstable net radiative feedback, largely due to reduced upward SW radiation (i.e., an increase in absorbed solar radiation that exceeds the increase in OLR). The extent to which these radiative responses are out of the range of GCM simulated feedbacks depends in part on whether one considers the input SST as the relevant temperature change or the output surface air temperature: ACE2 and cBottle have weak increases in OLR and weak surface air warming. Further research on interpreting the controlling factors for the ML model radiative fluxes and how they accord with physical understanding would be instructive (cf. Hafner et al. (2025)).

Based on the analyses presented in this study, it is evident that NeuralGCM’s hybrid design, which combines a dynamical core with neural-network-based parameterizations, more closely matches well understood physical responses to warming. Its structure also enables it to reproduce dynamically consistent responses, such as amplified upper-tropospheric warming and strengthened westerlies. In contrast, the cBottle and ACE2 design of “whole-model” emulators that infer the full atmospheric state directly from boundary forcing do not extrapolate to perturbed climates when trained on reanalysis states. The extent to which physical constraints beyond the global-mean conservation laws used in ACE2’s architecture can improve generalization is an important question for advancing the physical realism and robustness of next-generation ML climate models.

One motivation for the model comparison performed here is to establish a baseline of how well current model architectures and training strategies generalize to the out-of-sample climate changes of interest. To that end, it is valuable to examine both the overall response in quantities of interest and the inter-variable dependencies, which motivated our analysis of variables like column water vapor and the meridional circulation that are known to affect precipitation. Inter-variable relationships have also recently been used as part of the architecture for ML weather prediction (Fan et al., 2025). It is a challenge to solely use the reanalysis-era for training to build a model that captures the response to SST warming, though there are efforts to design climate-invariant ML approaches that have been successful for parameterizations in idealized simulations (Beucler et al., 2024; Liu & O’Gorman, 2025) and to develop coarse-grained, physically informed models (Falasca, 2025).

Our results highlight the promise of ML models as complementary tools to physical models for climate research, such as the precipitation response to warming. Identifying the tradeoffs between the low computational cost and fidelity of the response is an important validation step for current ML global atmospheric models. Uniform SST warming experiments provide a tractable and informative benchmark for ML models simulating climate change. There is the potential for significant progress from today’s frontier to improve their robustness and reliability in applications involving future climate change scenarios.

Methods

ML Models

In this study, we examine three global ML atmospheric models. They are:

1. **Climate in a Bottle, cBottle:** cBottle is a generative diffusion model developed by NVIDIA (Brenowitz et al., 2025). It consists of two complementary diffusion models: a coarse-generation model and a super-resolution model. While the super-resolution model version is useful for mesoscale weather and climate features, we exclusively evaluate the coarse model here. The coarse-generation model produces outputs at a resolution of approximately 100 km, comparable to that of typical CMIP6-era climate models (Eyring et al., 2016). This makes it a suitable tool for conducting multi-year climate emulation and investigating the large-scale response to SST perturbations. It is trained on ERA5 over the years 1980-2017. Atmospheric variables, such as wind and temperature, are represented on 8 pressure levels. cBottle takes monthly mean SST as input and generates hourly climate outputs, including the SST itself. It is distinctive in that it is not auto-regressive: the state of the atmosphere does not depend on its history. In this study, we conduct both the control and +2 K simulations for 10 years each, using the default set of diagnostic variables listed in Brenowitz et al. (2025). The monthly SST used in the control simulation is taken from the AMIP simulations that are part of the CMIP6 project (Eyring et al., 2016), with climatological values computed for the period 1981–2014. Note that cBottle allows control of stochastic variability through a user-defined “seed” parameter. In the simulations presented in the manuscript, this parameter was not specified. However, we performed two additional pairs of control and +2 K experiments with the seed set to 42 and 52, respectively, and found the results to be consistent, indicating that the results are robust and not sensitive to the seed setting.
2. **ACE2-ERA5:** ACE2-ERA5 is an auto-regressive ML model that uses Spherical Fourier Neural Operator architecture and is trained to emulate the global atmosphere by learning from the ERA5 reanalysis dataset (Watt-Meyer et al., 2025). It employs a two-stage architecture consisting of a convolutional encoder and a Transformer-based predictor with mass and water vapor conservation blocks to generate rollouts of key atmospheric variables, such as temperature, winds, and precipitation. Input and output variables for ACE2 can be found in supporting information in Watt-Meyer et al. (2025). ACE2-ERA5 operates on a regular latitude–longitude grid with 1° spatial resolution and 6-hourly temporal resolution, comparable to reanalysis products and suitable for weather-to-climate scale applications. There are 8 vertical layers in ACE2. The model can produce stable multi-year simulations when initialized with real-world atmospheric states and forced with observed sea surface temperatures (SSTs). ACE2-ERA5 uses SST and sea ice as forcing data to do the emulation and advances the atmospheric state over 6-hour steps. The 6-hourly SST and sea-ice forcing data is a coarsened version of the ERA5 reanalysis. We conduct both the control and +2 K simulations for 10 years each, using the default set of diagnostic variables listed in Watt-Meyer et al. (2025). Climatological values for the control simulation are computed over the period 1981–2014. Note that CO₂ concentration is also included as an input to ACE2-ERA5; however, we keep the CO₂ value identical in both the control and +2 K simulations. ACE2-ERA5 requires an initial condition, with available years including 1940, 1950, 1979, 2001, and 2020. Here, we use the initial condition from the year 2001 for both the control and +2 K experiments, with CO₂ concentration is about 370 ppm. Note that the overall performance is insensitive to the choice of initial conditions.
3. **NeuralGCM** is a hybrid ML model, combining a differentiable dynamical core with neural network parameterizations of all physical processes (Kochkov et al., 2024).

As such, NeuralGCM is not a whole model emulator like ACE2-ERA5 and cBottle. NeuralGCM has been shown to produce skillful medium-range forecasts and multi-year climate simulations. When forced with prescribed SSTs, NeuralGCM achieves stable decadal-scale simulations at resolutions of 140–280 km, capturing essential climate features such as seasonal cycles, tropical cyclone statistics, and large-scale circulation patterns. We save daily outputs for NeuralGCM, which has a time-step governed by the dynamical core (i.e., comparable to GCMs). An updated version of NeuralGCM includes precipitation as an output variable (Yuval et al., 2024), and we use this version of NeuralGCM to examine the response of precipitation along with other variables to uniform SST warming. Note that NeuralGCM can occasionally go unstable. We found this to be the case when using the climatological SST that we used for the ACE2 roll-out with 2 K of warming. For NeuralGCM, we used the ERA5 SST climatology over 2000-2020 (to better match its 2001-2018 training period), which was stable for 10 years for both the Control and +2 K simulations. All results presented here are based on these 10-year integrations. We also found that the public release of this precipitation version of NeuralGCM had long-term drifts that eventually went unstable when using NVidia H100, H200, and L40S Graphical Processing Units and consequently performed these rollouts on Google’s Colab platform with v6e-1 Tensor Processing Unit hardware.

In all cases, the input to the ML models was an SST climatology, rather than the interannually varying SST fields typically used in the Atmospheric Model Intercomparison Protocol (AMIP). A preliminary investigation suggests this choice does not substantially affect the results and allows for the shorter 10 year comparisons presented here.

Atmospheric General Circulation Model

We conduct simulations using the AM4 general circulation model, developed by the Geophysical Fluid Dynamics Laboratory (GFDL). Model descriptions of AM4 can be found in (Zhao et al., 2018a, 2018b). Briefly, AM4 features a cubed-sphere dynamical core with 96×96 grid cells per face, corresponding to an approximate horizontal resolution of 100 km. For analysis and comparison, model output is post-processed and re-gridded onto a regular latitude–longitude grid with 180 meridional points and 288 zonal points, yielding a resolution of 1.0° latitude \times 1.25° longitude. The model includes comprehensive physical parameterizations, including moist convection, radiation, cloud physics, and boundary layer turbulence. The control simulation is forced with monthly climatological sea surface temperatures (SSTs) and sea ice concentrations averaged over the period 1981–2014. To evaluate the model’s response to warming, we perform a uniform SST warming experiment with a +2 K anomaly applied globally over the ocean surface.

While we present the results of a single atmospheric GCM, we note that the amip protocol with uniform SST warming is an experiment in the Cloud Feedbacks Model Intercomparison protocol (Webb et al., 2017). There, the perturbation is 4 K, and we opted to evaluate a smaller magnitude perturbation so that the ML models were closer to their training data. The response of GCMs is typically approximately linear in the perturbation amplitude and it appears that ACE2-ERA5’s surface air temperature response is linear in SST perturbations (Watt-Meyer et al., 2025).

Observations

Global Precipitation Climatology Project, GPCP, v3.2 (Huffman et al., 2023) is used to evaluate the mean precipitation climatology. Radiation at the top of the atmosphere from CERES EBAF Edition 4.2.1 (NASA/LARC/SD/ASDC, 2024) is used to evaluate the models’ energy budget. Monthly ERA5 reanalysis data (Hersbach et al., 2020) is used for the surface air temperature.

Table 1. Comparison of ML models and AM4

Model	Spatial Resolution	Temporal Resolution of Output	Type	Output Variables Analyzed
cBottle [coarse]	100 km	hourly	Generative ML	tas, pr, column water vapor, u, v, t, OLR, SW up
ACE2-ERA5	100 km	6-hourly	Autoregressive ML	tas, pr, evaporation (surface latent heat flux), column water vapor, u, v, t, OLR, SW up
NeuralGCM	280 km	customizable	Hybrid ML-GCM	t1000, pr, evaporation, specific humidity (to compute column water vapor), u, v, t
AM4	100 km	customizable	Physics-based GCM	full atmospheric diagnostics

Author contributions

BZ and TM designed the study, conducted the machine-learning model experiments, and performed the analysis. BZ prepared the figures and TM contributed to the interpretation of the results. BZ and TM jointly discussed the findings and co-wrote the manuscript. All authors read and approved the final manuscript.

Acknowledgments

We thank Spencer Clark, Will Gregory, and Paul O’Gorman for helpful discussions. We thank Janni Yuval for disclosing NeuralGCM’s hardware-dependent behavior and constructive suggestions for how to address this. Simulations presented here were performed using High Performance Computing resources provided by the Cooperative Institute for Modeling the Earth System, with help from the Princeton Institute for Computational Science and Engineering. We acknowledge support from the National Oceanic and Atmospheric Administration, U.S. Department of Commerce under award NA23OAR4320198. The statements, findings, conclusions, and recommendations are those of the author and do not necessarily reflect the views of the National Oceanic and Atmospheric Administration, or the U.S. Department of Commerce.

Competing interests

All authors declare no financial or non-financial competing interests.

Data availability

The simulations were conducted and archived on Princeton’s computing system. The datasets generated and analyzed during the current study are available in the <https://tigris-web.princeton.edu/~bosongz/emulators/>.

Code availability

The cBottle code is available at <https://github.com/NVlabs/cBottle>, ACE2-ERA5 at <https://github.com/ai2cm/ace>, NeuralGCM at <https://neuralgcm.readthedocs.io/en/latest/index.html>, and AM4 at <https://github.com/NOAA-GFDL/AM4>. The code for generating figures for this study can be accessed via this link <https://tigris-web.princeton.edu/~bosongz/emulators/code/>.

References

- Allen, M. R., & Ingram, W. J. (2002). Constraints on future changes in climate and the hydrologic cycle. *Nature*, *419*, 224–232.
- Baxter, I., Pahlavan, H., Hassanzadeh, P., Rucker, K., & Shaw, T. (2025). Benchmarking atmospheric circulation variability in an AI emulator, ACE2, and a hybrid model, NeuralGCM. *arXiv preprint arXiv:2510.04466*.
- Beucler, T., Gentine, P., Yuval, J., Gupta, A., Peng, L., Lin, J., ... others (2024). Climate-invariant machine learning. *Science Advances*, *10*(6), eadj7250.
- Bi, K., Xie, L., Zhang, H., Chen, X., Gu, X., & Tian, Q. (2023). Accurate medium-range global weather forecasting with 3d neural networks. *Nature*, *619*(7970), 533–538.
- Bloch-Johnson, J., Rugenstein, M. A., Alessi, M. J., Proistosescu, C., Zhao, M., Zhang, B., ... others (2024). The green’s function model intercomparison project (gf mip) protocol. *Journal of Advances in Modeling Earth Systems*, *16*(2), e2023MS003700.

- Bordoni, S., Kang, S., Shaw, T. A., Simpson, I., & Zanna, L. (2025). The futures of climate modeling. *npj Climate and Atmospheric Science*, 8(1), 99.
- Bracco, A., Brajard, J., Dijkstra, H. A., Hassanzadeh, P., Lessig, C., & Monteleoni, C. (2025). Machine learning for the physics of climate. *Nature Reviews Physics*, 7(1), 6–20.
- Brenowitz, N. D., Ge, T., Subramaniam, A., Gupta, A., Hall, D. M., Mardani, M., . . . Pritchard, M. S. (2025). Climate in a bottle: Towards a generative foundation model for the kilometer-scale global atmosphere. *arXiv preprint arXiv:2505.06474*.
- Bretherton, C. S., Henn, B., Kwa, A., Brenowitz, N. D., Watt-Meyer, O., McGibbon, J., . . . Harris, L. (2022). Correcting coarse-grid weather and climate models by machine learning from global storm-resolving simulations. *J. Adv. Model. Earth Syst.*, 14(2), e2021MS002794.
- Bretherton, C. S., Peters, M. E., & Back, L. E. (2004). Relationships between water vapor path and precipitation over the tropical oceans. *J. Climate*, 17, 1517–1528.
- Byrne, M. P., & O’Gorman, P. A. (2013a). Land-ocean warming contrast over a wide range of climates: Convective quasi-equilibrium theory and idealized simulations. *J. Climate*, 26, 4000–4016.
- Byrne, M. P., & O’Gorman, P. A. (2013b). Link between land-ocean warming contrast and surface relative humidities in simulations with coupled climate models. *Geophys. Res. Lett.*
- Cess, R. D., Potter, G. L., Blanchet, J.-P., Boer, G. J., Del Genio, A. D., Deque, M., . . . others (1990). Intercomparison and interpretation of climate feedback processes in 19 atmospheric general circulation models. *J. Geophys. Res.*, 95, 16601–16615.
- Chapman, W. E., Schreck, J. S., Sha, Y., Gagne II, D. J., Kimpara, D., Zanna, L., . . . Berner, J. (2025). Camulator: Fast emulation of the community atmosphere model. *arXiv preprint arXiv:2504.06007*.
- Clark, S. K., Watt-Meyer, O., Kwa, A., McGibbon, J., Henn, B., Perkins, W. A., . . . Bretherton, C. S. (2024). ACE2-SOM: Coupling an ml atmospheric emulator to a slab ocean and learning the sensitivity of climate to changed CO₂. *arXiv preprint arXiv:2412.04418*.
- D’Agostino, R., Lionello, P., Adam, O., & Schneider, T. (2017). Factors controlling hadley circulation changes from the last glacial maximum to the end of the 21st century. *Geophysical Research Letters*, 44(16), 8585–8591.
- Dheeshjith, S., Subel, A., Adcroft, A., Busecke, J., Fernandez-Granda, C., Gupta, S., & Zanna, L. (2025). Samudra: An ai global ocean emulator for climate. *Geophysical Research Letters*, 52(10), e2024GL114318.
- Eyring, V., Bony, S., Meehl, G. A., Senior, C. A., Stevens, B., Stouffer, R. J., & Taylor, K. E. (2016). Overview of the coupled model intercomparison project phase 6 (CMIP6) experimental design and organization. *Geosci. Model Dev.*, 9, 1937–1958.
- Eyring, V., Gentine, P., Camps-Valls, G., Lawrence, D. M., & Reichstein, M. (2024). Ai-empowered next-generation multiscale climate modelling for mitigation and adaptation. *Nature Geoscience*, 17(10), 963–971.
- Falasca, F. (2025). Neural models of multiscale systems: conceptual limitations, stochastic parametrizations, and a climate application. *arXiv preprint arXiv:2506.22552*.
- Fan, H., Xiao, Y., Qu, Y., Ling, F., Fei, B., Bai, L., & Gentine, P. (2025). Incorporating multivariate consistency in M-based weather forecasting with latent-space constraints. *arXiv preprint arXiv:2510.04006*.
- Hafner, K., Iglesias-Suarez, F., Shamekh, S., Gentine, P., Giorgetta, M. A., Pincus, R., & Eyring, V. (2025). Interpretable machine learning-based radiation emulation for ICON. *Journal of Geophysical Research: Machine Learning and*

- Computation*, 2(4), e2024JH000501.
- Hartmann, D. L., & Larson, K. (2002). An important constraint on tropical cloud-climate feedback. *Geophys. Res. Lett.*, 29, 1951. (doi:10.1029/2002GL015835)
- Held, I. M., & Soden, B. J. (2006). Robust responses of the hydrological cycle to global warming. *J. Climate*, 19, 5686–5699.
- Hersbach, H., Bell, B., Berrisford, P., Hirahara, S., Horányi, A., Muñoz-Sabater, J., ... others (2020). The ERA5 global reanalysis. *Quart. J. Roy. Meteor. Soc.*, 146, 1999–2049.
- Huffman, G. J., Adler, R. F., Behrangi, A., Bolvin, D. T., Nelkin, E. J., Gu, G., & Ehsani, M. R. (2023). The new version 3.2 global precipitation climatology project (gpcp) monthly and daily precipitation products. *Journal of Climate*, 36(21), 7635–7655.
- Jeevanjee, N., & Romps, D. M. (2018). Mean precipitation change from a deepening troposphere. *Proc. Nat. Acad. Sci.*, 115, 11465–11470.
- Joshi, M. M., Gregory, J. M., Webb, M. J., Sexton, D. M. H., & Johns, T. C. (2008). Mechanisms for the land/sea warming contrast exhibited by simulations of climate change. *Clim. Dyn.*, 30, 455–465.
- Keisler, R. (2022). Forecasting global weather with graph neural networks. *arXiv preprint arXiv:2202.07575*.
- Kochkov, D., Yuval, J., Langmore, I., Norgaard, P., Smith, J., Mooers, G., ... others (2024). Neural general circulation models for weather and climate. *Nature*, 632(8027), 1060–1066.
- Kuo, Y.-H., Neelin, J. D., Chen, C.-C., Chen, W.-T., Donner, L. J., Gettelman, A., ... others (2020). Convective transition statistics over tropical oceans for climate model diagnostics: Gcm evaluation. *Journal of the Atmospheric Sciences*, 77(1), 379–403.
- Kushner, P. J., Held, I. M., & Delworth, T. L. (2001). Southern hemisphere atmospheric circulation response to global warming. *J. Climate*, 14, 2238–2249.
- Lam, R., Sanchez-Gonzalez, A., Willson, M., Wirnsberger, P., Fortunato, M., Alet, F., ... others (2023). Learning skillful medium-range global weather forecasting. *Science*, 382(6677), 1416–1421.
- Landsberg, J. B., & Barnes, E. A. (2025). Forecasting the future with yesterday’s climate: Temperature bias in AI weather and climate models. *arXiv preprint arXiv:2509.22359*.
- Lionello, P., D’Agostino, R., Ferreira, D., Nguyen, H., & Singh, M. S. (2024). The hadley circulation in a changing climate. *Annals of the New York Academy of Sciences*, 1534(1), 69–93.
- Liu, S., & O’Gorman, P. A. (2025). CERA: A framework for improved generalization of machine learning models to changed climates. *arXiv preprint arXiv:2509.00010*.
- Merlis, T. M., Cheng, K.-Y., Guendelman, I., Harris, L., Bretherton, C. S., Bolot, M., ... Fueglistaler, S. (2024). Climate sensitivity and relative humidity changes in global storm-resolving model simulations of climate change. *Sci. Adv.*, 10, eadn5217.
- NASA/LARC/SD/ASDC. (2024, 12 2). *Ceres energy balanced and filled (ebaf) toa monthly means data in netcdf edition4.2.1*. NASA Langley Atmospheric Science Data Center DAAC. Retrieved from https://doi.org/10.5067/TERRA-AQUA-NOAA20/CERES/EBAF-TOA_L3B004.2.1
- Neelin, J. D., Martinez-Villalobos, C., Stechmann, S. N., Ahmed, F., Chen, G., Norris, J. M., ... Lenderink, G. (2022). Precipitation extremes and water vapor: Relationships in current climate and implications for climate change. *Current Climate Change Reports*, 8(1), 17–33.
- O’Gorman, P. A., & Schneider, T. (2009a). The physical basis for increases in precipitation extremes in simulations of 21st-century climate change. *Proc. Nat. Acad. Sci.*, 106, 14773–14777.

- O’Gorman, P. A., & Schneider, T. (2009b). Scaling of precipitation extremes over a wide range of climates simulated with an idealized GCM. *J. Climate*, *22*, 5676–5685.
- Rackow, T., Koldunov, N., Lessig, C., Sandu, I., Alexe, M., Chantry, M., ... others (2024). Robustness of AI-based weather forecasts in a changing climate. *arXiv preprint arXiv:2409.18529*.
- Rasp, S., Hoyer, S., Merose, A., Langmore, I., Battaglia, P., Russell, T., ... others (2024). Weatherbench 2: A benchmark for the next generation of data-driven global weather models. *Journal of Advances in Modeling Earth Systems*, *16*(6), e2023MS004019.
- Santer, B. D., Wigley, T. M. L., Mears, C., Wentz, F. J., Klein, S. A., Seidel, D. J., ... others (2005). Amplification of surface temperature trends and variability in the tropical atmosphere. *Science*, *309*, 1551–1556.
- Vecchi, G. A., & Soden, B. J. (2007). Global warming and the weakening of the tropical circulation. *Journal of Climate*, *20*(17), 4316–4340.
- Watt-Meyer, O., Dresdner, G., McGibbon, J., Clark, S. K., Henn, B., Duncan, J., ... others (2023). Ace: A fast, skillful learned global atmospheric model for climate prediction. *arXiv preprint arXiv:2310.02074*.
- Watt-Meyer, O., Henn, B., McGibbon, J., Clark, S. K., Kwa, A., Perkins, W. A., ... Bretherton, C. S. (2025). Ace2: accurately learning subseasonal to decadal atmospheric variability and forced responses. *npj Climate and Atmospheric Science*, *8*(1), 205.
- Webb, M. J., Andrews, T., Bodas-Salcedo, A., Bony, S., Bretherton, C. S., Chadwick, R., ... others (2017). The cloud feedback model intercomparison project (CFMIP) contribution to CMIP6. *Geosci. Model Dev.*, *10*, 359–384.
- Wu, E., Rebassoo, F., Paul, P., Proistosescu, C., Nugent, J., McCoy, D., ... Bretherton, C. S. (2025). Applying the ace2 emulator to sst green’s functions for the e3smv3 global atmosphere model. *arXiv preprint arXiv:2505.08742*.
- Yuval, J., Langmore, I., Kochkov, D., & Hoyer, S. (2024). Neural general circulation models optimized to predict satellite-based precipitation observations. *arXiv preprint arXiv:2412.11973*.
- Zhang, B., Zhao, M., & Tan, Z. (2023). Using a green’s function approach to diagnose the pattern effect in gfdl am4 and cm4. *Journal of Climate*, *36*(4), 1105–1124.
- Zhao, M., Golaz, J.-C., Held, I., Guo, H., Balaji, V., Benson, R., ... others (2018a). The gfdl global atmosphere and land model am4. 0/lm4. 0: 1. simulation characteristics with prescribed ssts. *Journal of Advances in Modeling Earth Systems*, *10*(3), 691–734.
- Zhao, M., Golaz, J.-C., Held, I., Guo, H., Balaji, V., Benson, R., ... others (2018b). The gfdl global atmosphere and land model am4. 0/lm4. 0: 2. model description, sensitivity studies, and tuning strategies. *Journal of Advances in Modeling Earth Systems*, *10*(3), 735–769.